Journal of the European Ceramic Society 15 (1995) 1213–1220

0955-2219(95)00099-2
0955-2219/95/$9.50

The Solubility of Aluminium in Rare Earth Nitrogen Melilite Phases

K. S. Chee,[a] Y.-B. Cheng[a] & M. E. Smith[b]

[a]Department of Materials Engineering, Monash University, Melbourne, VIC 3168, Australia
[b]CSIRO Division of Materials Science and Technology, Melbourne, VIC 3168, Australia and Department of Physics, University of Kent, Canterbury CT2 7NR, UK

(Received 10 March 1995; revised version received 12 May 1995; accepted 31 May 1995)

Abstract

The incorporation of Al into nitrogen (N-)melilite phases has recently been reported [Cheng and Thompson, J. Am. Ceram. Soc., *77, 143–48 (1994)]. This occurrence allows simultaneous substitution of Al and O through replacement of Al–O for Si–N bonds and therefore, may offer potential improvement to the oxidation resistance properties of original N-melilite, which in the past was a problem that deterred the utilization of N-melilite as a grain boundary phase for Si_3N_4-based ceramics. In this work, the techniques of X-ray diffraction, scanning electron microscopy with quantitative energy dispersive X-ray spectroscopy and solid state ^{27}Al and ^{29}Si nuclear magnetic resonance spectroscopy with magic angle spinning have been used to study the solubility of Al in the structure of neodymium and samarium N-melilite phases.*

1 Introduction

N-melilites have the general formula $R_2Si_3O_3N_4$ (where R = yttrium or rare earth metals) and occur as an intermediate phase during the sintering of some Si_3N_4-based ceramics.[1] N-melilite has a tetragonal structure that is built up of an infinite linkage of corner-sharing $Si(O,N)_4$ units in tetrahedral sheets perpendicular to the [001] direction. Sandwiched between these sheets are Y^{3+} or rare earth Ln^{3+} ions which hold the silicon oxynitride layers together.[2] With a high nitrogen content of 67 eq%, N-melilite is very refractory; a melting point of ~1900°C has been quoted for yttrium N-melilite.[3] This feature alone makes N-melilite attractive as a grain boundary phase in Si_3N_4-based ceramics since the grain boundary phases control the high temperature performance of the materials, and grain boundary phases with superior thermal and chemical stability at elevated temperatures are highly sought after in Si_3N_4 materials research. Moreover, N-melilite is located in the phase compatibility regions of α and α–β SiAlONs, which in theory, can produce a good microstructure of SiAlONs with melilite as the only other secondary phase. These two characteristics of N-melilite combine to make it a potentially suitable grain boundary phase for Si_3N_4-based engineering ceramics. However, research in N-melilite has been slow coming primarily due to the poor reputation it has acquired during the early years of Si_3N_4 development. When yttria (Y_2O_3) was used in the 1970's as a sintering additive for Si_3N_4, a large number of silicon oxynitride phases emerged and N-melilite was one of them.[2] However, it was soon discovered that Si_3N_4 materials containing N-melilite had poor oxidation resistance with N-melilite oxidising rapidly at ~1000°C to form cristobalite and β-$Y_2Si_2O_7$.[3] The associated volume expansion of ~30% from the oxidation products caused extensive cracking of the ceramic component and presence of N-melilite has since been deemed undesirable.

Recent studies[4,5] have observed a significant solubility of Al in N-melilite phases resulting in a solid solution of the general formula, $R_2Si_{3-x}Al_xO_{3+x}N_{4-x}$ designated as M'_{ss}. In M'_{ss} phases, Si–N bonds are progressively being replaced by Al–O bonds as the Al solubility in the structure increases and this increase in oxygen content may provide a possible solution to the oxidation problem described above. M'_{ss} is gaining interest as a refractory grain boundary phase for SiAlON ceramics[6] with particular interest in the extent of Al solubility in M'_{ss} phases which will lead to a better understanding of their structure and properties and hence, the usefulness of these materials.

2 Experimental

Eight neodymium samples with the designed composition of $Nd_2Si_{3-x}Al_xO_{3+x}N_{4-x}$ (x = 0·0, 0·2, 0·6, 0·8, 1·0, 1·2, 1·4 and 2·0) along with two samarium

samples of composition $Sm_2Si_{3-x}Al_xO_{3+x}N_{4-x}$ (x = 0·2 and 1·0) were prepared from the starting powders of Si_3N_4 (Starck Berlin LC10), AlN (Starck Berlin Grade C), Al_2O_3 (Unilab) and Nd_2O_3 (CERAC), or Sm_2O_3 (Fluka) as appropriate. The surface oxide in both 'Si_3N_4' and 'AlN' was compensated using the calculated formulae of $Si_{2.823}N_{3.645}O_{0.177}$ for 'Si_3N_4' and $Al_{1.014}N_{0.985}O_{0.043}$ for 'AlN', which allow 4·0 wt% of SiO_2 for the Si_3N_4 powders and 3·5 wt% Al_2O_3 for the AlN powders. The pelletised powder mixes weighing approximately 3 g were placed into a BN-coated graphite crucible and sintered in an induction heating furnace with flowing nitrogen gas at 1700°C for 1 h. Weight loss of the samples after firing was less than 3 wt%.

The density of the sintered samples was determined by water immersion technique based on Archimedes Principle and all samples were boiled in water for 1 h prior to measurement. The crystalline phases were determined from powder X-ray diffraction (XRD) using a Rigaku Geigerflex diffractometer. Unit cell dimensions of the phases were calculated from the measured XRD peaks using a least square method[7] after calibration with Si as an internal standard. The actual Al content in the M'_{ss} phases was determined from quantitative EDXS using a ZAF correction method[8] with Y_2O_3 and elemental Al and Si as standards. The data was collected using a Jeol JSM-840 microscope operating at 10 kV and probe current of 1 nA with the final result being the mean of 10 experimental points. Micrographs of the phases were also taken with the Jeol JSM-840 operating in backscattered mode. MAS-NMR analysis was performed on a Varian VXR-600 spectrometer operating at 156·32 MHz for ^{27}Al and Bruker MSL-400 spectrometer operating at 79·47 MHz for ^{29}Si. The powdered samples were packed into conventional zirconia spinners and were spun at 12 and 4·5 kHz for ^{27}Al and ^{29}Si, respectively. ^{29}Si spectra were accumulated using 1·5 μs (tip angle ~30°) pulses with 15 s recycle delays while the corresponding conditions for ^{27}Al were 0·65 μs (15°) pulses and a 1–2 s recycle delay. ^{27}Al spectra were referenced against an external secondary standard of $Y_3Al_5O_{12}$ (AlO_6 = 0·7 ppm with respect to $[Al(H_2O)_6]^{3+}$). ^{29}Si MAS-NMR spectra were referenced to tetramethylsilane (TMS) at 0 ppm.

3 Results and Discussion

3.1 Weight loss and density

Compositions, weight loss and density of the neodymium samples after sintering at 1700°C for 1 h are shown in Table 1. There appears to be a trend whereby reduction in weight loss is accompanied by Al addition. The Al-free sample, N0 has a weight loss (ΔW) of 2·7% and this is reduced to 0·6% in the highest Al-containing sample, N20. All samples have a weight loss of < 3·0% which may in part be responsible for the relatively single-phase melilite samples obtained here since low weight loss is indicative of minimal changes to the starting composition during sintering. Density increases substantially with increasing Al addition, from 3·267 g/cm^3 in sample N0 to 4·618 g/cm^3 in sample N20. With increasing Al addition, the formation of a liquid phase which may possess a lower viscosity than the Al-free melilite composition is promoted, facilitating densification. The relatively high density of samples N14 and N20 may in part be due to the large amount of $NdAlO_3$ found in those samples since $NdAlO_3$ has a higher density than N-melilite.

3.2 Crystalline phases

The crystalline phases of the sintered samples as detected by X-ray diffraction (XRD) are shown in Table 1. Most of the samples except those with a high Al content produce almost single phase melilite with only trace amounts of apatite ($Nd_{10}(SiO_4)_6N_2$) and wollastonite ($NdSiO_2N$).

Table 1. Weight loss, density and crystalline phases of the sintered $Nd_2Si_{3-x}Al_xO_{3+x}N_{4-x}$ samples

Sample	*Designed Formula*	*X-value*	*ΔW(%)*	*D(g/cm³)*	*Crystalline phases as determined by XRD*				
					M	*M'ss*	*A*	*W*	*NdAlO₃*
N0	$Nd_2Si_3O_3N_4$	0·0	2·7	3·267	vs	—	w	mw	—
N2	$Nd_2Si_{2.8}Al_{0.2}O_{3.2}N_{3.8}$	0·2	2·0	3·696	—	vs	vw	mw	—
N6	$Nd_2Si_{2.4}Al_{0.6}O_{3.6}N_{3.4}$	0·6	1·4	3·611	—	vs	w	—	vw
N8	$Nd_2Si_{2.2}Al_{0.8}N_{3.8}N_{3.2}$	0·8	2·2	4·026	—	vs	vw	—	w
N10	$Nd_2Si_{2.0}Al_{1.0}O_{4.0}N_{3.0}$	1·0	1·1	4·335	—	vs	w	vw	m
N12	$Nd_2Si_{1.8}Al_{1.2}O_{4.2}N_{2.8}$	1·2	2·9	4·246	—	vs	vw	—	s
N14	$Nd_2Si_{1.6}Al_{1.4}O_{4.4}N_{2.6}$	1·4	1·6	4·451	—	s	ms	w	vs
N20	$Nd_2Si_{1.0}Al_{2.0}O_{5.0}N_{2.0}$	2·0	0·6	4·618	—	m	vw	—	vs

M = N-melilite ($Nd_2Si_3O_3N_4$); M'_{ss} = Al-containing N-melilite ($Nd_2Si_{3-x}Al_xO_{3+x}N_{4-x}$); A = apatite ($Nd_{10}(SiO_4)_6N_2$); W = wollastonite ($NdSiO_2N$).
X-Ray intensities: s = strong, m = medium, w = weak, v = very.

Neodymium N-melilite is detected in the Al-free sample N0, but from sample N2 onwards, the d-spacings for melilite phases continuously increase with Al addition indicating the formation of neodymium M'_{ss}. Similar to samarium and yttrium M'_{ss} phases,[4,5] the neodymium analogues do not display a different XRD pattern from that of Al-free N-melilite, implying a random solid solution with Al which does not alter the original melilite crystal structure. Apatite is observed in small amounts in all the sintered products and since there has been very little change in its lattice spacing, very limited Al, if any, is incorporated into the apatite structure.[9] Wollastonite is also detected in some of the samples. Neodymium wollastonite forms at a relatively low temperature and is unstable at high temperatures, melting at approximately 1700°C.[9] Slasor *et al.*[9] reported that wollastonite formation was dependent on firing schedule and with fast cooling, wollastonite did not appear. The wollastonite present here could have been retained during firing at 1700°C or it may have precipitated during the cooling process. Similar to apatite, neodymium wollastonite also exhibits limited Al solubility.[9] $NdAlO_3$, which is detected from sample N6 onwards forms readily and its concentration increases systematically with increasing Al content. In the Al-rich samples, N14 and N20, $NdAlO_3$ becomes the principal phase although M'_{ss} is still clearly present. A further increase in Al_2O_3 could only make $NdAlO_3$ so dominant that a reliable analysis for M'_{ss} phase become impossible. J-phase or the solid solution, J'_{ss} which was reported in the yttrium[5] and samarium[4] melilite-containing systems is not detected in any of the neodymium compositions produced in this work although neodymium J-phase is known to exist.[9]

Figure 1 shows the backscattered scanning electron microscopy (SEM), micrograph of sample N14 and quantitative energy dispersive X-ray spectroscopy (EDXS) spectra of the phases detected. SEM microstructural observation is in good agreement with phases identified by XRD. The EDXS spectrum of M'_{ss} clearly shows a substantial concentration of Al in this phase while for apatite, the Al peak is almost absent, indicative of negligible Al solubility. While atomic number contrast could not be distinguished between apatite and $NdAlO_3$ (both phases have a high neodymium concentration), EDXS is able to reveal that the smaller and relatively well-dispersed white regions are $NdAlO_3$ while apatite is significantly larger (Fig. 1).

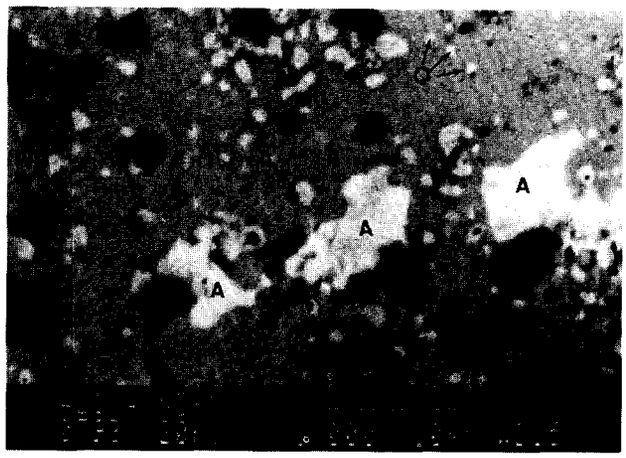

matrix = M'_{ss} A = apatite O = $NdAlO_3$

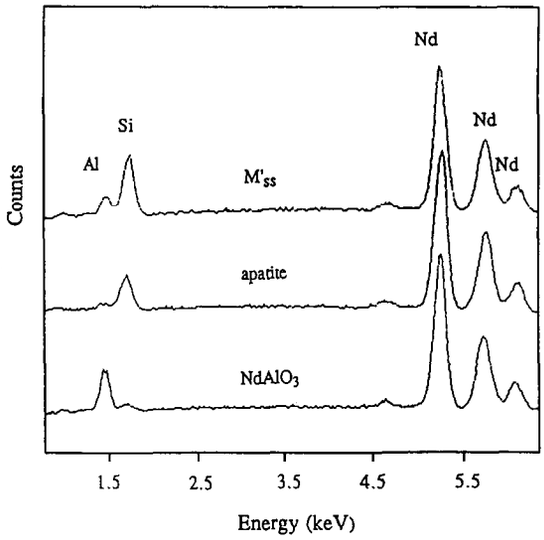

Fig. 1. Back-scattered SEM micrograph and EDXS spectra of sample N14.

3.3 Solubility of Al in neodymium M'_{ss}

Figure 2 shows the variation in the unit cell dimensions of neodymium M'_s as a function of starting x value in the designed composition, $Nd_2Si_{3-x}Al_xO_{3+x}N_{4-x}$. The starting x value ranging from 0·0 to 2·0 exhibits a relatively large expansion in both a and c lattices of the tetragonal M'_{ss} structure from x = 0·0 to about 1·0. Further increase in Al content beyond x = 1·0 produces a relatively smaller expansion rate indicating that the Al solubility of neodymium M'_{ss} is approaching saturation. A plot of cell dimension changes as a function of the measured amount of Al in the M'_{ss} phases as determined from quantitative EDXS is shown in Fig. 3 where, within the solubility limit the a and c lattices increase linearly with increasing Al according to the following equations:

$$a(\text{Å}) = 7{\cdot}719 + 0{\cdot}054x \quad (1)$$

$$c(\text{Å}) = 5{\cdot}032 + 0{\cdot}036x. \quad (2)$$

The above equations show a very similar lattice expansion to that exhibited by samarium M'_{ss}

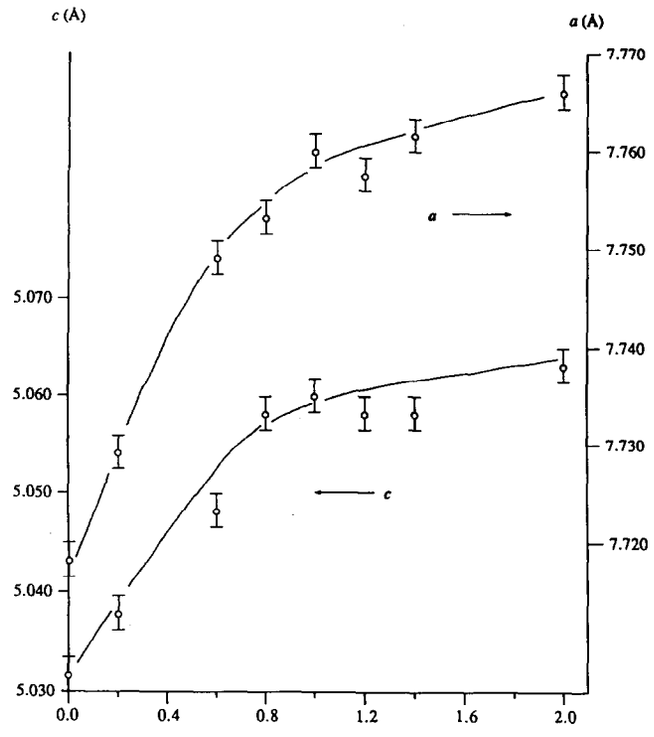

Fig. 2. Variation in the cell dimensions of neodymium M'_{ss} with starting x value.

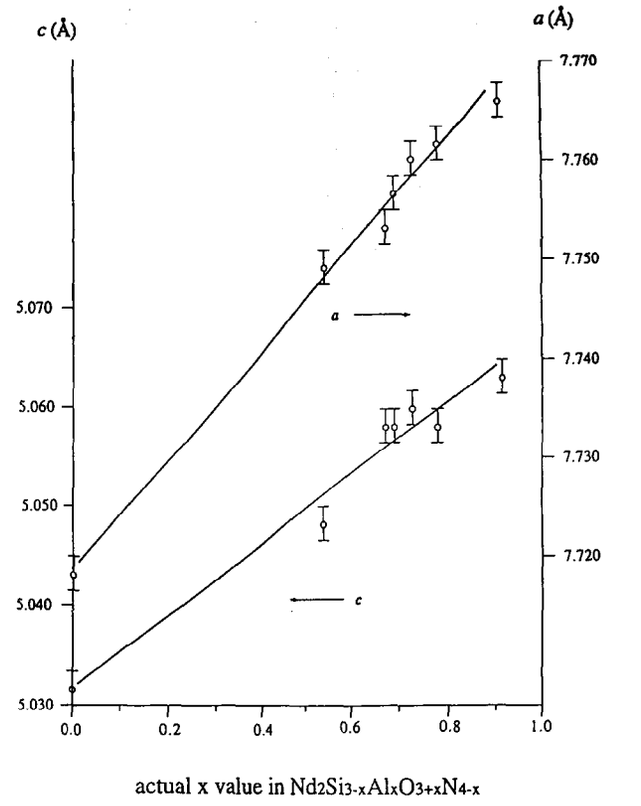

Fig. 3. Variation in the cell dimensions of neodymium M'_{ss} with actual x value determined from EDXS.

phases[4]. While both a and c lattices increase with Al addition, the calculated c/a ratio remains almost constant at 0·652 as shown in Table 2 indicating a random, uniform distribution of Al atoms within the M'_{ss} tetrahedral layers. Table 2 also provides a comparison between the designed x value and the actual Al concentration in M'_{ss} as determined by EDXS. Initially, most of the Al from the powder mixture is incorporated into M'_{ss} but as the composition further increased, discrepancy between the starting x and the actual x becomes larger. The maximum Al content obtained in neodymium M'_{ss} is $x = 0{\cdot}91$, implying that approximately one Si atom is replaced by an Al, therefore, giving a terminal composition of $Nd_2Si_{2\cdot0}Al_{1\cdot0}O_{4\cdot0}N_{3\cdot0}$.

The cell dimension measurements and EDXS analysis have clearly shown that neodymium M'_{ss} has a maximum Al solubility limit which is similar to that of samarium M'_{ss} phases[4] but higher than that of yttrium M'_{ss}.[5] It appears that the varying levels of Al substitution of different M'_{ss} phases may be related to the size of the interlayer cations. Table 3 is a compilation of experimental data on the formation of melilite phases in different systems with respect to the ionic radius of the cations. It is seen from Table 3 that there is a certain size criterion for N-melilite formation and in systems where the cation size is between ~0·9 and ~1·0 Å, N-melilite forms readily. If the cation radius is too big such as La^{3+} (1·016 Å) or too small as for Yb^{3+} (0·858 Å), N-melilite is not observed in those systems.

While the results shown in Table 3 are not conclusive, there seems to be a correlation between cation size and the maximum Al solubility limit where systems of relatively smaller cation sizes exhibit a significantly lower Al accommodation ability. Previous studies[4,5] have suggested that $x = 1{\cdot}0$ is the maximum Al solubility that can be accommodated by M'_{ss} phases without structural changes and it is seen from Table 3 that this limit has been achieved in the neodymium and samarium systems. Dy^{3+} and Y^{3+} which have ionic radii of 0·908 and 0·893 Å, respectively, have correspondingly lower Al solubility limits of $x = 0{\cdot}7$ and 0·6.

Table 2. Cell dimension calculations and EDXS measurements of the neodymium M'_{ss} samples

Sample	*Starting x-value*	*Actual x-value*	*Cell dimensions (Å) a (± 0·002) c (± 0·002)*		*c/a ratio*
N0	0·0	—	7·718	5·032	0·652
N2	0·2	[a]	7·729	5·037	0·652
N6	0·6	0·54	7·749	5·048	0·651
N8	0·8	0·67	7·753	5·058	0·652
N10	1·0	0·73	7·760	5·060	0·652
N12	1·2	0·69	7·757	5·058	0·652
N14	1·4	0·78	7·762	5·058	0·652
N20	2·0	0·91	7·766	5·063	0·652

[a]The actual Al content in this sample is too low to be reliably determined.

Table 3. Compilation of experimental data on the formation of N-melilite in different systems

Cation	*Ionic radius* r_R^{3+} (Å)[a]	$r_R^{+3}:r_O^{2-}$	*Al-free N-melilite formation*	*Formation of* M'_{ss}	*Maximum Al solubility in* M'_{ss}
La^{3+}	1·016	0·77	does not form [10]	no study	[b]
Nd^{3+}	0·995	0·75	observed[11]	observed	$x = \sim 1{\cdot}0$
Sm^{3+}	0·964	0·73	observed[11]	observed[4]	$x = \sim 1{\cdot}0$
Dy^{3+}	0·908	0·69	observed[11]	observed[12]	$x = \sim 0{\cdot}7$
Y^{3+}	0·893	0·68	observed (not at 1500°C)[11]	observed[5]	$x = \sim 0{\cdot}6$
Yb^{3+}	0·858	0·65	does not form [11,13]	no study	[b]

[a]Data from CRC Handbook of Chemistry and Physics, 72nd Edition, 1992.
[b]Experimental data currently unavailable.

Figure 4 is a schematic representation of the structure of yttrium melilite projection on (100). With non-bridging anions taking up position on the apex of the tetrahedra, each silicon oxynitride layer of the N-melilite structure possesses an overall negative charge that has to be balanced by the cations (e.g. Y^{3+}). These cations separate the silicon oxynitride layers by a finite distance. In systems with small cation sizes such as yttrium or dysprosium, the negatively charged layers are allowed to come relatively closer together and possibly create a repulsive force which may destabilise the melilite structure. A structurally unstable M'_{ss} phase may result in a low Al accommodation capability. The exact mechanism involved in this process is currently unknown but the size of the interlayer cations appears to play an important role in determining the level of Al substitution in M'_{ss} phases.

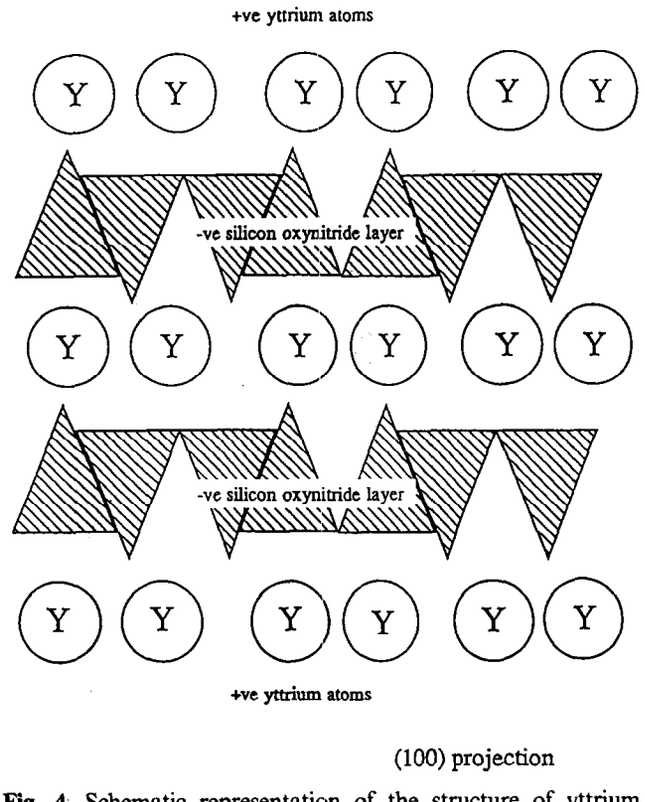

Fig. 4. Schematic representation of the structure of yttrium N-melilite showing the separation of the negatively charged silicon oxynitride layers by Y^{3+} cations.

3.4 ^{27}Al and ^{29}Si MAS-NMR data

Solid state ^{27}Al and ^{29}Si magic angle spinning NMR (MAS-NMR) were used to probe the Al and Si structural coordination in M'_{ss}. Paramagnetic ions possess unpaired electrons which produce large fluctuating magnetic field in the neighbourhood of the ions. The NMR signals from nearby nuclei can experience severe broadening, that for lanthanide stannates was found to be proportional to the square of the magnetic moment.[16] The unpaired electron can also produce a significant shift through the electron spin density being transferred onto the nucleus and is termed the Fermi contact shift. The magnitude of these effects depends on the relative orientation of the nuclei in the structure. This means that compared to diamagnetic analogues the NMR spectra may be much broader and show unconventional shift. Neodymium has a moderately large magnetic moment and contact shift[14] and it proved difficult to obtain NMR spectra from neodymium N-melilites. These effects are much smaller for samarium and NMR spectra could be obtained for samarium analogues. The two samarium samples prepared under identical conditions as those of the neodymium samples contain crystalline phases as shown in Table 4.

^{27}Al MAS-NMR spectra of the samarium samples, S2 ($x = 0{\cdot}2$) and S10 ($x = 1{\cdot}0$) are shown in Fig. 5(a) and (b), respectively. In Fig. 5(a) two resonances are observed, a sharp peak at 110 ppm and a much broader one centred at 55 ppm. From the literature, the 110 ppm resonance is attributed to AlN_4 coordination units.[15] However, it is unlikely that the substitution of Al–O for Si–N bonds in the melilite phase could lead to all Al in the AlN_4 coordination because this will cause charge imbalance in the solid solution. In addition, if some of the Al atoms are coordinated as AlN_4, there would have to be two distinct $Si_2(O,N)_7$ coordination in the M'_{ss} structure[15] but the present ^{29}Si NMR results could not strongly support this postulation (Fig. 6). The small area under the 110 ppm resonance is indicative of a very minor phase

Table 4. Weight loss, density and crystalline phases of the sintered $Sm_2Si_{3-x}Al_xO_{3+x}N_{4-x}$ samples

Sample	*Formula*	*x-value*	*ΔW(%)*	*D(g/cm³)*	*Crystalline phases as determined by XRD*		
					M'ss	*A*	*$SmAlO_3$*
S2	$Sm_2Si_{2.8}Al_{0.2}O_{3.2}N_{3.8}$	0·2	0·8	3·788	vs	w	—
S10	$Sm_2Si_{2.0}Al_{1.0}O_{4.0}N_{3.0}$	1·0	0·7	4·669	vs	w	m

M'_{ss} = Al-containing N-melilite ($Sm_2Si_{3-x}Al_xO_{3+x}N_{4-x}$); A = apatite ($Sm_{10}(SiO_4)_6N_2$).
X-Ray intensities: s = strong, m = medium, w = weak, v = very.

and previous studies[17] have attributed this peak to unreacted AlN which was beyond XRD detection. The other Al site in this sample is AlO_4 as represented by the resonance at 55 ppm. The much larger area under this peak suggests that it represents a structural unit of significant proportion. Since there are no Al-containing phases in sample S2 other than M'_{ss} according to XRD, this resonance must arise from the Al environment in the M'_{ss} structure. There are few signs of any paramagnetic broadening or shifting of these resonances which must be a result, at least for the N-melilite, of the orientation of the samarium and aluminium in the structure. The spectrum of S10 in Fig. 5(b) shows a principal resonance at 10 ppm which is attributed to AlO_6 units in $SmAlO_3$.[5] The strong intensity of this resonance corresponds to the XRD results which shows a significant amount of $SmAlO_3$ present in the sample. The ^{27}Al resonance from $SmAlO_3$ shows no noticeable shift from the position expected for AlO_6 units in such a structure, but there is an extensive envelope of broad sidebands which demonstrate the influence of the samarium ion. This indicates that the contact shift is small but the broadening effect marked. The peak at approximately 100 ppm is mainly the result of a spinning sideband which probably overlaps with a small amount of AlN_4 contribution. Similar to the low Al containing sample S2, sample S10 shows a clear peak at 55 ppm corresponding to AlO_4 coordination from M'_{ss}. A major difference between samarium and yttrium ^{27}Al spectra[16] is the absence of a well-defined 30 ppm resonance in the samarium samples. This confirms the correct assignment of the 30 ppm peak in the yttrium samples to the Al-containing J-phase (J'_{ss}) since samarium J'_{ss} does not form in the samples produced here hence, no corresponding 30 ppm or equivalent peaks are observed.

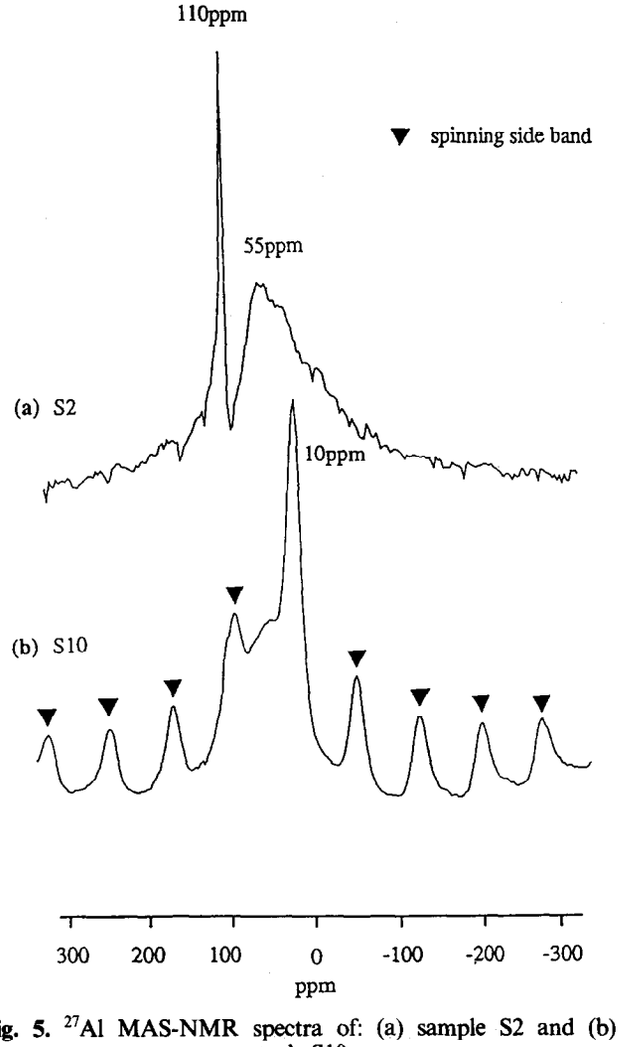

Fig. 5. ^{27}Al MAS-NMR spectra of: (a) sample S2 and (b) sample S10.

The ^{29}Si spectra of S2 and S10, shown in Figures 6(a) and (b) are very similar with both spectra producing a single resonance at approximately –35 ppm. The rest of the peaks in the two spectra are attributed to spinning sidebands and it appears that the Si environments in both low and high Al-containing samples are identical. Unlike yttrium silicon oxynitride compounds which have been extensively studied and a catalogue of ^{29}Si resonance positions defined,[18] phases in the samarium silicon oxynitride system have not been investigated by NMR and there is no reference to associate the ^{29}Si chemical shift values to particular Si environments. Apart from the 'normal' isotropic chemical shift, the resonance at –35 ppm also has an additional contact shift, further complicating peak assignment.[19] Obviously the fields produced by the Sm ion at the Al and Si sites in the M'_{ss} structure are slightly different. While the type of Si coordination which gives rise to the –35 ppm resonance is uncertain since this is not simply the chemical shift, the spectra provides unequivo-

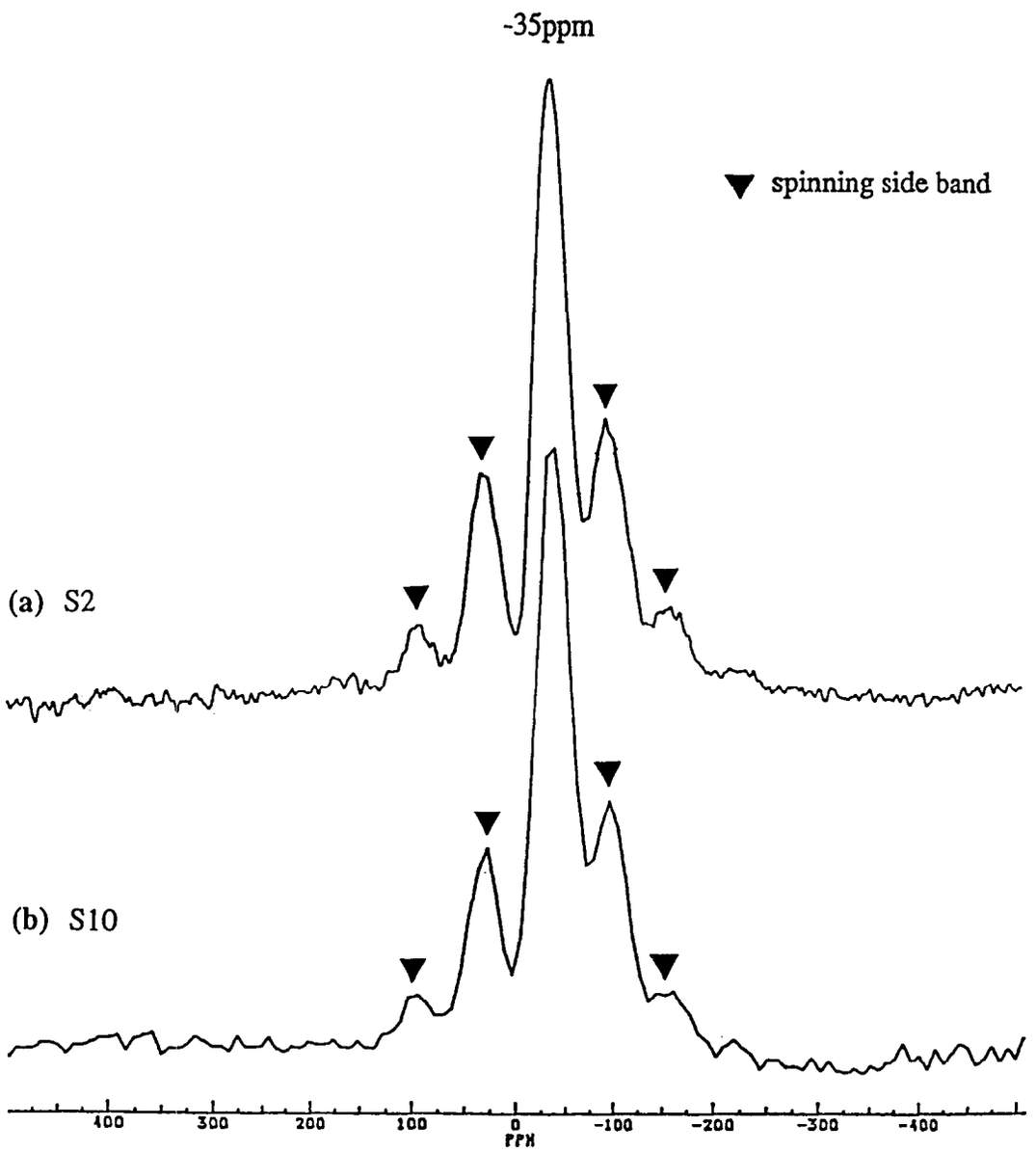

Fig. 6. ^{29}Si MAS-NMR spectra of: (a) sample S2 and (b) sample S10.

cal evidence that there is only one Si site in samarium M'_{ss} phases and by comparison with results from the yttrium system[16,18] the Si coordination in samarium M'_{ss} is more than likely to be SiO_2N_2.

From the ^{27}Al and ^{29}Si MAS-NMR data obtained, the predominant coordination's of Al and Si in samarium M'_{ss} are interpreted as AlO_4 and SiO_2N_2, respectively, and there is no evidence of transformation from one type of coordination to another with increasing Al solubility. The atomic arrangement of rare earth M'_{ss} is, therefore, similar to that proposed for yttrium M'_{ss}[16] where Al occupies the corner and centre positions of the M'_{ss} unit cell as shown in Fig. 7. From this model of atomic arrangement, the maximum number of Al atoms per unit cell will have to be two. This translates to an x value of 1·0 since two M'_{ss} chemical formulae of $R_2Si_{3-x}Al_xO_{3+x}N_{4-x}$ make up one unit cell, suggesting a terminal composition of $R_2Si_2AlO_4N_3$. This is in good agreement with the EDXS results described above where the maximum Al solubility for neodymium M'_{ss} approaches $x = 1{\cdot}0$.

4 Conclusions

There is a significant solubility of Al in neodymium M'_{ss} phases. A maximum of one Si can be replaced by Al giving the terminal composition of $Nd_2Si_2AlO_4N_3$. Cell dimension measurements and EDXS analysis have shown that neodymium M'_{ss} has a maximum Al solubility limit $x = 1$ in the formulae $Nd_2Si_{3-x}Al_xO_{3+x}N_{4-x}$, which is similar to that of samarium M'_{ss} phases but higher than that of yttrium M'_{ss}. This discrepancy is thought to be related to the size of the interlayer cations in the M'_{ss} structure. Structural investigation by MAS-NMR has suggested that samarium M'_{ss} phases consist predominantly of AlO_4 and SiO_2N_2 coordination units, regardless of the extent of Al solubility.

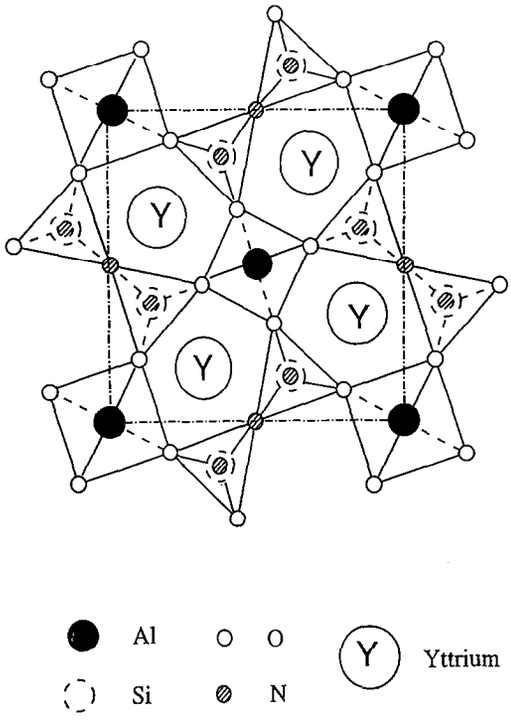

Fig. 7. Proposed atomic arrangement of yttrium M'_{ss} at the possible maximum Al solubility based on NMR results, after Ref. 18.

Acknowledgements

The authors wish to thank Dr T. J. Bastow from CSIRO Division of Materials Science and Technology for performing some of the NMR experiments. CSIRO is thanked for partial support and M. E. Smith thanks the SERC for access to the ultrahigh field facility at Edinburgh. K. S. Chee is a recipient of the Monash University Postgraduate Writing-Up Award.

References

1. Jack, K. H., Fabrication of dense nitrogen ceramics. In *Processing of Crystalline Ceramics*, eds H. Palmour III, R. F. Davis & T. M. Hane. Plenum Press, New York, (1978) pp. 561–78.
2. Jack, K. H., Review: sialons and related nitrogen ceramics. *J. Mater. Sci.*, **11** (1976) 1135–58.
3. Jack, K. H., Silicon nitride, sialons and related ceramics. In *Ceramics and Civilisation*, Vol III, *High-Technology Ceramics*. The American Ceramic Society, Columbus, OH, (1986) pp. 259–88.
4. Cheng, Y.-B. & Thompson, D. P., Aluminium-containing nitrogen melilite phases. *J. Am. Ceram. Soc.*, **77** (1994) 143–8.
5. Chee, K. S., Cheng, Y.-B., Smith, M. E. & Bastow, T. J., The solubility of aluminium in yttrium nitrogen melilite phases. In *Proceedings of the International Ceramic Conference Austceram 94*, eds C. C. Sorrell & A. J. Ruys. The Australian Ceramic Society, Sydney (1994). pp. 1031–6.
6. Cheng, Y.-B. & Thompson, D. P., Preparation and grain boundary devitrification of samarium α-sialon ceramics. *J. Eur. Ceram. Soc.*, **14**(7) (1994) 13–21.
7. Carr, A. J., *WEMAG* and *LATPAR* computer programs, University of Strathclyde, Glasgow (1989).
8. Ware, N. G., *S.P.E.E.D.* computer program, Australian National University, Canberra (1989).
9. Slasor, S., Liddell, K., and Thompson, D. P., The role of Nd_2O_3 as an additive in the formation of α' and β' sialons. In *Special Ceramics 8*, eds S. P. Howlett & D. Taylor. The Institute of Ceramics, Shelton, Staffordshire, UK, (1986) pp. 51–64.
10. Harris, R. K., Leach, M. J. & Thompson, D. P., Nitrogen-15 and oxygen-17 NMR spectroscopy of silicates and nitrogen ceramics. *Chem. Mater.*, **4** (1992) 260–7.
11. Wang, P. L., Sun, W. Y. & Yen, T. S., Formation and densification of *R*-α'-SiAlONs (R = Nd, Sm, Gd, Dy, Er and Yb). In *Silicon Nitride Ceramics: Scientific and Technological Advances*, Vol. 287. eds I.-W. Chen, P. F. Becher, M. Mitomo, G. Petzow & T.-S. Yen. Materials Research Society, (1993) pp. 387–92.
12. Yan, D.-S., Personal communication (1994).
13. Hoffman, M. J. & Petzow, G., Microstructural design of Si_3N_4 based ceramics. In *Silicon Nitride Ceramics: Scientific and Technological Advances*, Vol. 287. eds I.-W. Chen, P. F. Becher, M. Mitomo, G. Petzow & T.-S. Yen, Materials Research Society (1993) pp. 3–14.
14. Grey, C. P., Dobson, C. M., Cheetham, A. K. & Jakeman, R. J. B., Studies of rare-earth stannates by ^{119}Sn MAS NMR. The use of paramagnetic shift probes in the solid state. *J. Am. Chem. Soc.*, **111** (1989) 505–11.
15. Smith, M. E., Observation of mixed $Al(O,N)_4$ structural units by ^{27}Al magic angle spinning NMR. *J. Phys. Chem.*, **96** (1992) 1444–8.
16. Chee, K. S., Cheng, Y.-B. & Smith, M. E., NMR investigation on the structure of aluminium-containing yttrium nitrogen melilite (M'_{ss}). *Chem. Mater.*, in press.
17. Dupree, R., Lewis, M. H. & Smith, M. E., Structural characterisation of ceramic phases with high-resolution ^{27}Al NMR. *J. Appl. Cryst.*, **21** (1988) 109–16.
18. Dupree, R., Lewis, M. H. & Smith, M. E., High-resolution silicon-29 nuclear magnetic resonance in the Y–Si–O–N system. *J. Am. Chem. Soc.*, **110** (1988) 1083–7.
19. Grey, C. P., Smith, M. E., Cheetham, A. K., Dobson, C. M. & Dupree, R., ^{89}Y MAS NMR study of rare-earth pyrochores: paramagnetic shifts in the solid state. *J. Am. Chem. Soc.*, **112** (1990) 4670–5.